Mechanisms of Radiation Damage in Beam-Sensitive Specimens, for TEM Accelerating Voltages Between 10 and 300 kV

R.F. EGERTON*
Physics Department, University of Alberta, Edmonton, Canada T6G 2E1

KEY WORDS radiation damage; radiolysis; knock-on displacement; dose-limited resolution

ABSTRACT Ionization damage (radiolysis) and knock-on displacement are compared in terms of scattering cross section and stopping power, for thin organic specimens exposed to the electrons in a TEM. Based on stopping power, which includes secondary processes, radiolysis is found to be predominant for all incident energies (10–300 keV), even in materials containing hydrogen. For conducting inorganic specimens, knock-on displacement is the only damage mechanism but an electron dose exceeding 1000 C cm^{-2} is usually required. Ways of experimentally determining the damage mechanism (with a view to minimizing damage) are discussed. *Microsc. Res. Tech. 75:1550–1556, 2012.*

INTRODUCTION

The mechanism of radiation damage in beam-sensitive TEM specimens is of practical interest because it determines what options are available for minimizing the damage. If radiolysis is the main damage process, the use of a specimen holder cooled by liquid nitrogen or liquid helium can reduce the damage by typically a factor of 3–10 (Henderson, 1990; International Experimental Study Group, 1986). If knock-on displacement is predominant, reducing the TEM accelerating voltage below some threshold value will largely eliminate the damage. If the damaging effects arise from beam heating or from electrostatic charging of an insulating specimen, reducing the incident-beam current can be helpful.

Radiation damage limits the number of electrons that can be recorded from a small region of the specimen (size δ) to a value $N = F(D_c/e)\delta^2$, where F is the fraction of electrons that reach the detector, e is the electronic charge, and D_c the characteristic (or critical) electron dose (or fluence) that the specimen can tolerate without losing its structure. The recorded signal is CN, where C is the contrast relative to adjacent elements, and the associated shot noise is $N^{1/2}$, so the signal/noise ratio of the recorded signal is SNR = $(\mathrm{DQE})^{1/2}$ $(CN/N^{1/2})$, DQE being the detective quantum efficiency of the detector. Combining these two expressions gives an estimate of the dose-limited resolution:

$$\delta = (\mathrm{SNR})(\mathrm{DQE})^{-1/2}C^{-1}(FD_c/e)^{-1/2} \qquad (1)$$

Equation (1) applies also to spectroscopic measurements. For electron energy-loss spectroscopy (EELS), N represents the number of energy-loss electrons within the spectral region being analyzed. For energy-dispersive X-ray (EDX) spectroscopy, N is the number of photons within a characteristic peak, and F represents the number of such photons per incident electron.

According to Eq. (1), the spatial resolution for imaging or analysis of a beam-sensitive specimen can be improved by increasing DQE, C or F, parameters that depend partly on instrument design and are therefore within experimental control. However, the most variable factor in Eq. (1) is the characteristic dose, which depends on the specimen and its damage mechanism.

Damage may occur by radiolysis, arising from the inelastic scattering of incident electrons, in which case the degree of damage is usually assumed to be proportional to the energy deposited per unit volume of the specimen. Allowing for plural scattering in a specimen of thickness t, the average energy deposited per incident electron is $\langle E\rangle = (t/\lambda_i)E_m$, where E_m is the average energy loss per inelastic event and λ_i is the mean free path for all inelastic scattering (Egerton, 2011). Bethe theory gives $\lambda_i \propto v^2$, where v is the incident-electron speed, so the energy deposited is proportional to t/v^2 and the energy deposited per unit volume is proportional to $1/v^2$.However, a spectroscopy (EDX, EELS) signal is also a consequence of inelastic scattering and is proportional to t/v^2, while the elastic signal that gives rise to phase or diffraction contrast is proportional to t/v^2 if the specimen is very thin. According to these arguments, the signal/damage ratio is independent of v but proportional to t, so if the specimen thickness is reduced to accommodate a lower TEM accelerating voltage, the signal/damage ratio is compromised. More detailed analysis based on Eq. (1) suggests that the dose-limited resolution depends more on the imaging mode than on the accelerating voltage (Egerton, 2012). For example, phase contrast (achieved with a phase plate in the back-focal plane of a TEM objective lens) offers higher resolution than dark-field or bright-field TEM imaging.

*Correspondence to: R.F. Egerton, Physics Department, University of Alberta, Edmonton, Canada T6G 2E1. E-mail: regerton@ualberta.ca

Received 10 May 2012; accepted in revised form 20 June 2012

Contract grant sponsor: Natural Science and Engineering Research Council of Canada

DOI 10.1002/jemt.22099

Published online 17 July 2012 in Wiley Online Library (wileyonlinelibrary.com).

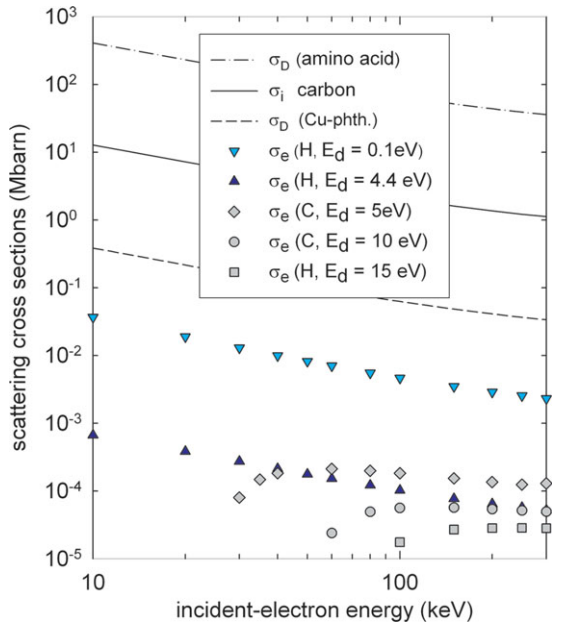

Fig. 1. Scattering cross sections appropriate to radiolysis (smooth curves) and knock-on displacement (discrete data points) for E_0 between 10 and 300 keV.

Damage can also occur as a result of high-angle elastic scattering, which gives rise to knock-on displacement of atoms within a specimen or ejection from a surface (electron-induced sputtering). In this case, the $1/v^2$ dependence of damage does not apply; for a given displacement energy, there is a threshold incident energy below which displacement cannot occur. Knock-on damage is predominant in conductors, where radiolysis is suppressed because of the high electron density. In such specimens, an accelerating voltage below the threshold value is desirable. If this threshold falls below 50 kV, however, a high accelerating voltage might actually be preferable, since the damage cross section starts to fall for voltages above about twice the threshold value (Rossell et al., 2009; Wang et al., 2011).

Recently there has been speculation that knock-on effects may be important in some nonconductors (soft materials or organic specimens), raising the possibility that low kV may be beneficial for these specimens. The main purpose of this study is to assess the extent of knock-on displacement in nonmetallic specimens (and therefore the kV-dependence of damage) by calculating cross sections and stopping powers appropriate to both radiolysis and displacement.

CROSS SECTIONS FOR RADIOLYSIS

The total cross section for inelastic scattering in a given material is:

$$\sigma_i = \int (d\sigma_i/dE)\, dE = (In_a t)^{-1} \int (dJ/dE) dE \qquad (2)$$

It can be determined by recording the energy-loss spectrum $J(E)$ from a thin specimen (thickness $t \ll \lambda_i$),

TABLE 1. Characteristic dose D_c, damage cross section σ_D (in Mb = 10^{-18} cm^2) and radiolytic efficiency $\eta = \sigma_D/\langle\sigma_i\rangle$ for some organic compounds (Pc denotes phthalocyanine) at E_0 = 100 keV (Reimer and Kohl, 2008)

Material	D_c (C cm^{-2})	σ_D (Mb)	$\sigma_D/\langle\sigma_i\rangle$
Glycine ($C_2H_5NO_2$)	0.0025	64	40
Paraffin ($C_{26}H_{28}$)	0.0080	20	13
Anthracene ($C_{14}H_{10}$)	0.1	1.6	1
Pc ($C_{32}H_{18}N_8$)	0.2	0.8	0.46
CuPc ($C_{32}H_{16}CuN_8$)	2.5	0.06	0.034
ClCuPc ($C_{32}H_2Cl_{14}CuN_8$)	20	0.008	0.0036

using an incident beam of intensity I. For elemental solids, σ_i may also be estimated from a simple atomic model (Lenz, 1954), values for carbon being shown in Figure 1. For an incident energy of E_0 = 100 keV, the Lenz model gives $\sigma_i = 2.1 \times 10^{-18}$ cm^2 = 2.1 Mbarn, equivalent to an inelastic mean free path of λ_i = 48 nm if ρ = 2 g cm^{-3} ($n_a = 1 \times 10^{23}$ cm^{-3}), comparable to measured values. On the log-log scale of Figure 1, the linear behavior at lower incident energy represents $\sigma_i \propto 1/E_0^{1/2}$; the curvature at higher E_0 is due to relativistic change in mass of the incident electrons.

Organic specimens contain various elements (H, N, O etc.) besides carbon, and an inelastic-scattering cross section per molecule σ_m can be estimated by summing the atomic cross sections. An average cross section per atom $\langle\sigma_i\rangle$ is obtained by dividing the cross section per molecule by the number of atoms per molecule. These cross sections do not directly represent the damage in organic specimens because not all inelastic collisions result in bond breakage, loss of structure or mass loss. Instead, the radiation sensitivity has to be found experimentally, from the fading of a diffraction pattern or disappearance of features in an energy-loss spectrum, for example. The characteristic dose D_c is taken as the dose at which a diffraction spot or spectral feature becomes invisible or falls by a factor of 2 or e (=2.72) from its original intensity. The reciprocal of D_c, having units of area, is referred to as a damage cross section σ_D; it is a direct measure of the radiation sensitivity of a material at a given incident-electron energy.

Damage cross sections for some simple organic compounds are shown in Table 1. The ratio $\eta = \sigma_D/\langle\sigma_i\rangle$ can be thought of as a radiolytic efficiency; $\eta < 1$ indicates that more than one inelastic collision per atom is needed to create damage. This situation holds for aromatic compounds such as anthracene or phthalocyanine (Pc), where delocalization of the π-electrons confers resonance stabilization within each molecule. The radiation stability is further enhanced by replacing all or most of the hydrogen atoms with a halogen (such as Cl), as seen in Table 1.

Large values of η are observed for aliphatic compounds, among the most sensitive being the aliphatic amino acids such as glycine. In this case, a single inelastic collision may destroy a whole molecule. The damage sensitivity is further increased by secondary processes: a secondary electron created from an inelastic collision of a primary electron can have many eV of kinetic energy, allowing it to travel through the specimen and undergo inelastic collisions that cause further damage. Assuming η to be independent of incident energy, damage cross sections for glycine and chlorinated copper phthalocyanine are given as dashed lines

in Figure 1. As shown in Table 1, most organic compounds fall between these two extremes.

CROSS SECTIONS FOR KNOCK-ON DISPLACEMENT

Knock-on displacement is believed to be the sole damage process in conducting specimens. Although inelastic scattering excites electrons from the conduction band and from inner shells, the high density of conduction electrons ensures that electron vacancies (holes) are filled within a time (<1 fs) short compared to an atomic-vibration period (≈100 fs). De-excitation can then occur without atom displacement or other radiolysis effects.

Knock-on damage arises from the elastic scattering of a primary electron, which transfers energy directly to an atomic nucleus, by an amount E that depends on the scattering angle θ:

$$E = E_{\max}\sin^2(\theta/2) = (E_{\max}/2)(1-\cos\theta) \qquad (3)$$

Here $E_{\max}$ is the maximum possible energy exchange, corresponding to a head-on collision (θ =180°), and given by

$$E_{\max}(\mathrm{eV}) = (2/A)(m_0/u)E_0(2+E_0/m_0c^2) = (1.1/A)(2+E_0/m_0c^2)E_0(\mathrm{keV}) \qquad (4)$$

where A is the atomic weight (mass number) of the scattering atom, u is the atomic mass unit (1.66×10^{-27} kg), and m_0c^2 = 511 keV is the electron rest energy. As shown by Eq. (3), a scattering angle of at least 90° is necessary to give $E > E_{\max}/2$. For the low-angle scattering that forms most of the TEM diffraction pattern, $E < E_{\max}/300$ and these electrons do not cause displacement.

There is a threshold incident energy E_0^{th}, below which displacement damage is absent because $E_{\max} < E_{\mathrm{d}}$, where E_{d} is the bulk or surface displacement energy of the scattering atom. In practical terms,

$$E_0^{\mathrm{th}} = (511\ \mathrm{keV})\{[1+AE_{\mathrm{d}}/(561\ \mathrm{eV})]^{1/2}-1\} \qquad (5)$$

For most elemental solids, E_0^{th} is above 200 keV for bulk displacement but below 200 keV for surface sputtering. In fact, E_0^{th} is below 100 keV for many low-Z atoms, which has provided impetus for the development of TEM instrumentation that operates well at lower accelerating voltage. For example, atomic-scale imaging has been demonstrated with aberration-corrected monochromated TEMs operating at 40 kV (Bell et al., 2012) and 20 kV (Kaiser et al., 2011).

Because atomic displacement requires the elastic collision to take place very close to an atomic nucleus, the screening effect of atomic electrons is unimportant and the angle-differential cross section is given fairly well by the Rutherford formula: $\mathrm{d}\sigma_e/\mathrm{d}\Omega = 4\gamma^2Z^2/(a_0^2q^4)$ where $q = 2k_0\sin(\theta/2)$ is the scattering wavenumber and k_0 the wavenumber of the incident electron. Because scattering angle and energy loss are linked by Eq. (3), this formula can be integrated over energy loss rather than scattering angle, giving a displacement cross section:

$$\sigma_{\mathrm{d}} = \frac{\pi\gamma^2Z^2}{a_0^2k_0^4}\int_{E_{\min}}^{E_{\max}}\frac{E_{\max}}{E^2}\,\mathrm{d}E = (0.25\ \mathrm{barn})\,F(v)\,Z^2\left[\frac{E_{\max}}{E_{\min}}-1\right] \qquad (6)$$

where $F(v) = \gamma^{-2}(v/c)^{-4} = (1 - v^2/c^2)(v/c)^{-4}$ (=7.75 at E_0 = 100 keV), $E_{\min} = E_{\mathrm{d}}$ and $E_{\max}$ is given by Eq. (5).

Displacement energies for organic materials are not well known; E_{d} will depend on the type of bonding and whether the atom lies in the interior or at the surface of a specimen. The C—C bond energy being 3.5 eV and C=C bond energy 6.24 eV, a carbon displacement energy of E_{d} = 5 eV has been used in the past. However, each carbon atom has several bonds and E_{d} is said to be as high as 22 eV in single-layer graphene (Meyer et al, 2012).

In Figure 1, Eq. (6) has been used to compute σ_{d} for carbon atoms with displacement energies of 5, 10, and 15 eV, which probably spans the entire range of organic compounds. The cross sections fall to zero at threshold incident energies E_0^{th} that lie between 20 and 100 keV, so C-atom displacement can be avoided by using a sufficiently low incident-electron energy. However, the displacement cross sections are a factor of 10^2 to 10^5 lower than the damage cross sections for radiolysis, so this advantage appears insignificant.

Hydrogen is a rather special case: its low nuclear mass results in a threshold energy below 2 keV, according to Eq. (5). The C—H bond energy is 4.36 eV and the corresponding displacement cross sections are given by the triangular data points in Figure 1. They are almost a factor of 10^3 lower than the radiolysis cross section for copper phthalocyanine. In some materials, H atoms are involved in hydrogen bonding and E_{d} may be as low as 0.1 eV, giving displacement cross sections (inverted triangles in Fig. 1) within a factor of 10 of the radiolysis cross section for copper phthalocyanine. On this basis, it appears that knock-on displacement of hydrogen might contribute appreciably to the damage in some organic compounds.

However, scattering cross sections make no allowance for secondary damage. In the case of knock-on displacement, this means that a displaced atom may travel within the specimen and cause further knock-on damage. In the case of radiolysis, it means that secondary electrons produced by inelastic scattering cause further ionization damage, which forms the rationale for expressing the damaging effect of ionizing radiation in units of Gray (Gy): Joules of energy deposited per kg of material. In both cases, the secondary processes can be incorporated by assuming that the damage is proportional to the amount of energy absorbed from primary electrons, which is represented by the stopping power of the specimen. We should therefore re-evaluate radiolysis and knock-on displacement in terms of their associated stopping powers.

STOPPING POWER FOR RADIOLYSIS

Energy deposition arising from inelastic scattering can be expressed in terms of an electronic stopping

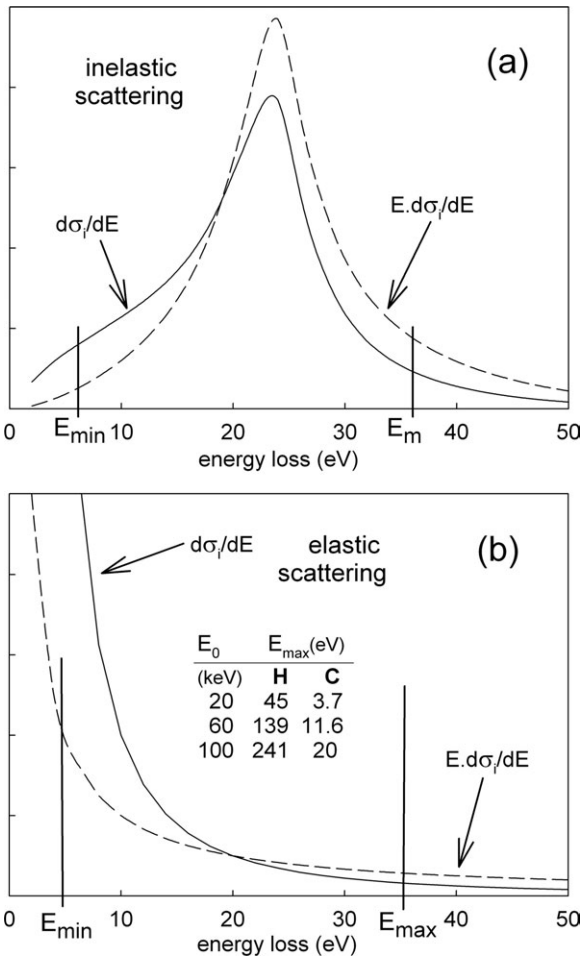

Fig. 2. **a**: Energy-loss dependence of the differential cross section for inelastic scattering ($d\sigma_i/dE$) and of the related stopping power, with the energy scale appropriate to a typical organic compound. **b**: Energy-loss dependence of the differential cross section for elastic scattering: $(d\sigma_e/dE) \int E^{-2}$, and the corresponding stopping power: $E(d\sigma_e/dE) \int E^{-1}$, with integration limits (E_{min} and E_{max}) appropriate to displacement damage.

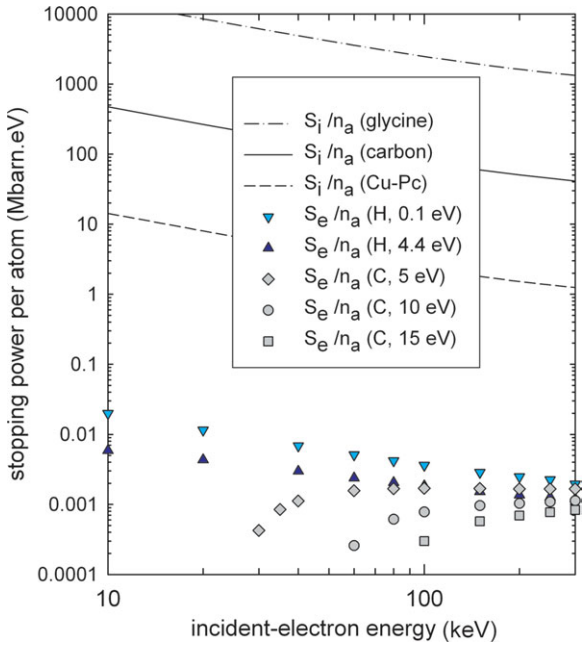

Fig. 3. Stopping cross sections for radiolysis (smooth curves) and knock-on displacement (discrete data points) for E_0 between 10 and 300 keV.

power: $S_i = dE/dz$, which is the energy deposited per unit distance z as an electron travels through the specimen and is related to the differential cross section ($d\sigma_i/dE$) by:

$$S_i = n_a \int E(d\sigma_i/dE)\, dE = n_a E_m \sigma_i = E_m/\lambda_i \qquad (7)$$

Here $n_a = \rho/(uA)$ represents the number of atoms per unit volume of the specimen (density ρ) and the integration is over all energy loss. E_m is a mean energy loss per inelastic collision, taking into account all inelastic processes, including innershell excitation. For carbon, K-shell excitation accounts for about 30% of the stopping power (Egerton et al., 2012), resulting in $E_m \approx 37$ eV for an organic compound (Isaacson, 1979). Taking that value and $\lambda_i = 100$ nm (typical for an organic material at $E_0 = 100$ keV), $S_i = 3.7$ eV cm^{-1} and Eq. (7) shows that a dose (fluence) of 0.01 C cm^{-2} is equivalent to a dose of 30 MGy if $\rho = 1$ g cm^{-3}. The stopping power per atom S_i/n_a is also known as a stopping cross section and has units energy $\times$ area.

In practice, not all energy losses cause ionization damage. There is a threshold value (E_{min} in Fig. 2a) below which bond breakage does not occur, but this threshold is low: about 4.8 eV in PMMA (Lin, 1975). The upper limit of integration is set by the beam energy E_0, but $E_0 \gg E_m$ for TEM irradiation. Therefore the damage is approximately represented by a total integral, as in Eq. (7).

Making use of Eq. (7) and taking $E_m = 37$ eV, the E_0-dependence of the stopping cross section for elemental carbon is given by the solid curve in Figure 3. Damage cross sections σ_D for organic compounds are based on measured values of characteristic dose and therefore include secondary processes. The dashed curves in Figure 3 give the stopping cross section for glycine and copper phthalocyanine, assuming that $E_m \approx 37$ eV and that σ_D/σ_i is independent of E_0. Because E_m does not vary with incident energy, the E_0-dependences in Figure 3 are the same as those in Figure 1.

Secondary processes are important in radiolysis damage, where the mean energy loss (e.g., 37 eV) is much higher than the threshold energy (e.g., 5 eV), suggesting that secondary electrons carry away a large part of the deposited energy. In poly(methyl methacrylate), it is believed that 80% the electron-irradiation damage arises from secondary electrons (Wu and Neureuther, 2001). In very thin (<10 nm) specimens, the percentage will be lower because a significant fraction of the secondaries can escape into the vacuum (Pennycook and Howie, 1980).

TABLE 2. Maximum (N_{max}) and mean (N_{mean}) numbers of secondary displacements (atom 2) following a single displacement (atom 1) by electrons of kinetic energy E_0

E_0 (keV)	Atom 1	E_{max} (eV)	E_m (eV)	Atom 2	N_{max}	N_{mean}	P_{mean} (%)
40	C (5 eV)	7.6	6.1	C (5 eV)	1	1	0.02
				H (4.4 eV)	0	0	0
				H (0.1 eV)	21	17.4	0.32
	H (4.4 eV)	91	14	C (5 eV)	5	0.8	0.02
				H (4.4 eV)	20	3.2	0.07
				H (0.1 eV)	914	140	3.0
	H (0.1 eV)	91	0.7	C (5 eV)	5	0.04	0.04
				H (4.4 eV)	20	0.16	0.16
				H (0.1 eV)	914	6.8	6.8
300	C (5 eV)	71	14	C (5 eV)	14	2.9	0.04
				H (4.4 eV)	4	0	0
				H (0.1 eV)	202	41	5.3
	C (10 eV)	71	23	C (10 eV)	7	2.3	0.01
				H (4.4 eV)	4	1.5	0.01
				H (0.1 eV)	202	64	0.32
	H (4.4 eV)	854	23	C (5 eV)	48	1.3	0.01
				H (4.4 eV)	194	5.3	0.03
				H (0.1 eV)	8,537	233	1.2
	H (0.1 eV)	854	0.9	C (5 eV)	48	0.05	0.01
				H (4.4 eV)	194	0.2	0.05
				H (0.1 eV)	8,537	9.1	2.1

The displacement energy of each atom is given in parentheses after its chemical symbol. The last column gives the rate of each secondary process: $P_{mean}(\%) = 100\, N_{mean}\sigma_d J$, where σ_d is the primary-displacement cross section in barn and $J = 1.6 \times 10^5$ A cm^{-2}. Values in the last two columns are likely to be overestimates, since they assume a head-on collision of the two atoms.

STOPPING POWER FOR KNOCK-ON DISPLACEMENT

Knock-on damage can also involve secondary processes (Cosslett, 1978). Measured damage cross sections are scarce but we can deduce the stopping power by calculation. Use of the Rutherford cross section gives the following expression for the stopping cross section:

$$S_e/n_a = \int E(d\sigma_e/dE)\, dE = (0.25 \text{ barn})F(v)Z^2E_{max}\log_e(E_{max}/E_{min}) \quad (8)$$

where E_{max} is given by Eq. (4) and $E_{min} = E_d$ as before. Values for carbon and hydrogen atoms are given in Figure 3, using previous values of the displacement energy. The most obvious difference, compared to the scattering cross sections shown in Figure 1, is that the displacement of weakly bound (0.1 eV) hydrogen appears much less significant; for example, compare the inverted triangles with the upright triangles representing strongly bound (4.36 eV) hydrogen. The elastic-scattering cross section appears high for a weakly bound H atom due to contributions from energy losses between 0.1 and 4.36 eV, but these add little to the stopping power because of the E-weighting within the integral in Eq. (8).

The role of secondary processes in displacement damage can be further evaluated as follows. For a knock-on process, $d\sigma_e/dE \propto E^{-2}$ leads to a mean energy loss of the primary electron given by

$$E_m = E_{max}\, \log_e(E_{max}/E_{min})[E_{max}/E_{min} - 1]^{-1} \quad (8)$$

For displacement of weakly bound hydrogen, E_m is below 1 eV (see Table 2), so most of the ejected H atoms can displace other H atoms but not C atoms.

According to nonrelativistic mechanics, the initially displaced atom (atomic weight A_1, kinetic energy E_1) can transfer to a neighboring stationary atom (atomic weight A_2, displacement energy E_{d2}) a maximum energy equal to $E_2 = 4E_1[A_1A_2/(A_1+A_2)^2]$. Therefore the maximum possible number of secondary displacements is:

$$N_{max} = 4(E_{max}/E_{d2})[A_1A_2/(A_1 + A_2)^2] \quad (9)$$

Likewise, the average number of secondary displacements can be estimated as:

$$N_{mean} = 4(E_m/E_{d2})[A_1A_2/(A_1 + A_2)^2] \quad (10)$$

Equation (10) will actually provide an overestimate, since it assumes that the momentum supplied by the primary electron is directed toward the nearest-neighbor atom 2, so that atom 1 makes a head-on collision.

Results of applying Eqs. (9) and (10) to weakly and strongly bound C and H atoms are given in Table 2. Large numbers (N_{max}) of secondary displacements are possible when hydrogen atoms are involved, particularly if they are weakly bound (0.1 eV). However, the *average* number (N_{mean}) of secondary displacements is considerably less; most collisions of the primary electron involve $\theta < 180^\circ$, so the mean energy transfer E_m is much less than E_{max}. Even so, more than a hundred secondary displacements might occur if atom 1 is strongly bound to carbon and atom 2 is part of a weak hydrogen bond.

While N_{mean} is an estimate of secondary displacement relative to the primary one, the last column in Table 2 gives a rough measure of the absolute probability of each secondary event per second ($P_{mean} = N_{mean}\sigma_d J$), for an incident intensity of $J = 10^{24}$ e cm^{-2} (1.6×10^5 A cm^{-2}), which is readily obtainable in an aberration-corrected TEM probe. The H-atom cross section σ_d is about 50 times larger for a weakly bound atom but the mean energy loss E_m is 20–25 times smaller, giving a stopping power only about twice that of strongly bond hydrogen; see Figure 3 and the last column of Table 2.

INORGANIC SPECIMENS

In inorganic solids, both knock-on and radiolysis effects can take place, sometimes simultaneously. Radiolysis is predominant in insulators such as halides, oxides, hydrides, hydroxides, sulfides and silicates (Hobbs, 1984). The temperature dependence can be complex (Hobbs, 1975) but lower temperature usually means less change to the specimen.

In conducting samples, radiolysis is largely quenched, leaving knock-on displacement as the damage mechanism. Although the primary displacement is largely independent of sample temperature, secondary processes such as defect aggregation are often thermally activated. Therefore a TEM with a variable-temperature specimen holder can be useful for studying the details of damage and simulating the effects of β-irradiation, for example in ceramics or glasses intended as radioactive-waste storage (Lian et al,

TABLE 3. Characteristic dose D_c (=e/σ_d for knock-on) and the proposed damage mechanism for a few inorganic materials, measured for specimens at room temperature

Specimen	E_0 (keV)	D_c (C cm^{-2})	Reference	Mechanism
Zeolite	100	0.1–1.0	Pan and Crozier (1993)	Radiolysis
NaCl	100	80	Hobbs (1975)	Radiolysis
C_{60}	100; 200	500; 780	Egerton and Takeuchi (1999)	Radiolysis
Au	500; 1,000	530; 100	Cherns et al. (1976)	Knock-on sputtering
TiC; Cr_2N	100; 100	4×10^5; 1.3×10^5	Thomas (1985)	Knock-on sputtering
C (amor.); Al	300; 300	1.3×10^4; 2×10^3	Egerton et al. (2010)	Knock-on sputtering
Graphene	100; 200	8×10^5; 1.2×10^4	Meyer et al. (2012)	Knock-on sputtering

2009). As in the case of organic materials, cross sections for knock-on displacement are generally smaller than for radiolytic damage and the characteristic dose correspondingly larger; see Table 3.

Even in an elemental solid such as carbon, details of the damage process can be somewhat complex. In single-layer graphene, molecular-dynamics calculations predict a C-displacement energy of 22 eV (Kotakoski et al., 2010), which would give $I_0^{th} = 109$ keV according to Eq. (5). The observed threshold is at about 85 keV and the discrepancy has been explained as being due to out-of-plane (zero-point) vibrations of the C atoms (Meyer et al., 2012). For carbon nanotubes, E_d depends on the tube diameter and the angle between the incident electron and the surface; $E_0^{th} \approx 86$ keV for perpendicular incidence and $E_0^{th} > 139$ keV for electrons travelling nearly parallel to the surface (Smith and Luzzi, 2001; Zobelli et al., 2007). In solid C_{60} (fullerite), a dose of <0.1 C cm^{-2} causes polymerization, in the form of crosslinking between adjacent molecules (Tada and Kanayama, 1996). However, about 500 C cm^{-2} is needed to destroy the phenyl rings present in each molecule, as judged by 100 keV EELS measurements of the 6.5 eV peak (Egerton and Takeuchi, 1999) and 9,000 C cm^{-2} is required for substantial loss of diffraction spots due to the displacement of molecules (Seraphin et al., 1993).

CONCLUSIONS

For organic specimens in the TEM, radiolysis is the predominant damage mechanism and secondary effects (due to secondary electrons) account for a major part of this damage. The threshold incident energy for knock-on displacement of carbon is below 100 keV but this process contributes little to the stopping power and the resulting damage, even at higher incident energies. Knock-on displacement of hydrogen can be significant in terms of scattering cross section but not in terms of stopping power, since most of the ejected H atoms have low kinetic energy and create little secondary damage.

As a consequence, it does not appear likely that incident energies (10–100 keV) below the carbon knock-on threshold are favorable in terms of reducing the damage, unless new contrast mechanisms appear. In aromatic compounds, a threshold effect for radiolysis has been reported and linked to the requirement for K-shell excitation (Howie, 1985; Isaacson, 1972) but the threshold incident energy is below 1 keV and therefore not applicable to TEM operation.

Inorganic specimens damage by knock-on displacement or by radiolysis, or both. Radiolysis predominates in insulators and knock-on damage in conducting specimens. Because the knock-on cross sections are relatively small, the damage mechanism can sometimes be inferred from the dose D_c needed to create damage. For incident energies between 100 and 300 keV, $D_c <$ 1,000 C cm^{-2} suggests radiolysis whereas $D_c >$ 1,000 C cm^{-2} suggests knock-on displacement; see Table 3.

Other ways of distinguishing between these two mechanisms are through the incident-energy and temperature dependence. For radiolysis, D_c increases with E_0 (ideally by a factor of 2 between 100 and 300 keV) and increases with decreasing temperature (typically by a factor of 3 or more between 300 and 100 K). For knock-on displacement from a surface (electron-beam sputtering), D_c decreases with increasing E_0 (as seen in Table 3) and varies little with temperature. Bulk-displacement energies for crystalline solids are mostly above 20 eV, giving threshold energies above 200 keV.

Other specimen-damage mechanisms include electron-beam heating and electrostatic charging. For polymers, these two effects can combine to locally soften the specimen and tear it apart through electrostatic forces. Both effects depend on incident-current density, so reducing the beam current in the TEM can be helpful, even if the image or spectrum requires a longer recording time. As a result of secondary-electron emission, the irradiated area of a thin specimen charges positively. The external electric field can deflect the electron beam, while the internal field can cause migration of ions (Jiang and Silcox, 2002) or dielectric breakdown leading to specimen thinning or hole formation (Cazaux, 1995).

In view of the importance of radiation damage in electron microscopy and spectroscopy, it is to be hoped that this topic will receive renewed attention in the future. Modern instrumentation allows direct TEM imaging of displacement damage and STEM aloof-beam spectroscopy (Garcia de Abajo and Howie, 1999; Howie, 1983), in addition to the more traditional diffraction-pattern and EELS studies. It should even be feasible to position a STEM probe away from the nucleus of an atom (thereby avoiding displacement damage) but within the delocalization length for inelastic scattering, and thereby extract an inelastic signal that contains useful structural information (Krivanek et al., 2012).

ACKNOWLEDGMENTS

The author thanks Prof. Archie Howie and Prof. Ute Kaiser for valuable comments.

REFERENCES

Bell DC, Russo CJ, Kolmykov DV. 2012. 40 keV atomic resolution TEM. Ultramicroscopy 114:31–37.

Cazaux J. 1995. Correlations between ionization radiation effects in transmission electron microscopy. Ultramicroscopy 60:411–425.

Cherns D, Minter FJ, Nelson RS. 1976. Sputtering in the high voltage electron microscope. Nucl Instrum Meth 132:369–376.
Cosslett VE. 1983 Radiation damage in the high resolution electron microscopy of biological materials: A review. J Microsc 113:113–129.
Egerton RF. 2011. Electron energy-loss spectroscopy in the electron microscope,3rd ed. New York: Springer. p.171.
Egerton RF. Control of radiation damage in the TEM. Ultramicroscopy (in press).
Egerton RF, Takeuchi M. 1999. Radiation damage to fullerite (C_{60}) in the transmission electron microscope. Appl Phys Lett 75:1884–1886.
Egerton RF, McLeod R, Wang F, Malac M. 2010. Basic questions related to electron-induced sputtering in the TEM. Ultramicroscopy 110:991–997.
Egerton RF, Lazar S, Libera M. 2012. Delocalized radiation damage in polymers. Micron 43:2–7.
Garcia de Abajo FJ, Howie A. 1999. Electron spectroscopy from outside—Aloof beam or near field? Inst Phys Conf Ser 161:327–330.
Henderson R. 1990. Cryo-protection of protein crystals against radiation damage in electron and X-ray diffraction. Proc R Soc Lond B 241:6–8.
Hobbs LW. 1975. Transmission electron microscopy of extended defects in alkali halide crystals. In: Surface and Defect Properties of Solids, Roberts MW, Thomas JM, editors. London: The Chemical Society. p.152.
Hobbs LW. 1984. Radiation effects in analysis by TEM. In: Chapman JN, Craven AJ, editors. Quantitative electron microscopy. Edinburgh: SUSSP Publications. pp. 399–445.
Howie A. 1983. Surface reactions and excitations. Ultramicroscopy 11:141–148.
Howie A, Rocca FJ, Valdre U. 1985. Electron beam ionization damage processes in *p*-terphenyl. Phil Mag B 52:751–757.
International Experimental Study Group. 1986. Cryoprotection in electron microscopy. J Microsc 141:385–391.
Isaacson M. 1972. Interaction of 25 keV electrons with the nucleic acid bases, adenine, thymine, and uracil. II. Inner shell excitation and inelastic scattering cross sections. J Chem Phys 56:1813–1818.
Isaacson M. 1979. Electron beam induced damage or organic solids: Implications for analytical electron microscopy. Ultramicroscopy 4:193–199.
Jiang N, Silcox J. 2002. Electron irradiation induced phase decomposition in alkaline earth multi-component oxide glass. J Appl Phys 92:2310–2316.
Kaiser U, Biskupek J, Meyer JC, Leschner J, Lechner L, Rose H, Stöger-Pollach M, Khlobystov AN, Hartel P, Müller H, Haider M, Eyhusen S, Benner G. 2011. Transmission electron microscope at 20 kV for imaging and spectroscopy. Ultramicroscopy 111:1239–1246.
Krivanek OL, Zhou W, Chisholm MF, Dellby N, Lovejoy TC, Ramasse QM, Idrobo JC. 2012. Gentle STEM of single atoms: Low keV imaging and analysis at ultimate detection limits. In: Bell D, Erdman N, editors. Low voltage electron microscopy: Principles and applications. Oxford: Royal Microscopical Society (in press).
Kotakoski J, Jin CH, Lehtinen O, Suenaga K, Krasheninnikov AV. 2010. Electron knock-on damage in hexagonal boron nitride monolayers. Phys Rev B 82:113404.
Lian J, Wang LM, Sun K, Ewing RC. 2009. In situ TEM of radiation effects in complex ceramics Microsc Res Tech 72:165–181.
Lin BJ. 1975. Deep UV lithography. J Vac Sci Technol 12:1317–1320.
Lenz F. 1954. Zur Streuung mittelschneller Elektronen in kleinste Winkel. Z Naturforsch 9A:185–204.
Meyer JC, Eder F, Kurasch S, Skakalova V, Kotakoski J, Park HJ, Roth S, Chuvilin A, Eyhusen S, Benner G, Krasheninnikov AV, Kaiser U. 2012. An accurate measurement of electron beam induced displacement cross sections for single-layer graphene. Phys Rev Lett 108:196102.
Pan M, Crozier PA. 1993. Low dose high resolution electron microscopy of zeolite materials with slow scan CCD camera. Ultramicroscopy 48:332–340.
Pennycook SJ, Howie A. 1980. Study of single-electron excitations by electron microscopy II. Cathodoluminescence image contrast from localized energy transfers. Phil Mag 41:809–827.
Reimer L, Kohl H. 2008. Transmission electron microscopy. New York: Springer.
Rossell MD, Erni R, Asta M, Radmilovic, Dahmen U. 2009 Atomic resolution imaging of lithium in Al_3Li precipitates. Phys Rev B 80:024110.
Seraphin S, Zhou D, Jiao J. 1993. Electron-beam-induced structural changes in crystalline C_{60} and C_{70}. J Mater Res 8:1895–1899.
Smith BW, Luzzi DE. 2001. Electron irradiation effects in single wall carbon nanotubes. J Appl Phys 90:3509–3515.
Tada T, Kanayama T. 1996. Nanolithography using fullerene films as an electron beam resist. Jpn J Appl Phys 35:L63–L65.
Thomas LE. 1985. Light-element analysis with electrons and X-rays in a high-resolution STEM. Ultramicroscopy 18:173–184.
Wang F, Graetz J, Moreno MS, Ma C, Wu L, Volkov V, Zhu Y. 2011. Chemical distribution and chemical bonding of lithium in intercalated graphite: Identification with optimized electron energy loss spectroscopy. ACS Nano 5:1190–1197.
Wu B, Neureuther J. 2001. Energy deposition and transfer in electron-beam lithography. Vac Sci Technol B 19:2508–2511.
Zobelli A, Gloter A, Ewels CP, Seifert G, Colliex C. 2007. Electron knock-on cross section of carbon and boron nitride nanotubes. Phys Rev B 75:245402.